AIAA JOURNAL
Vol. 44, No. 12, December 2006

Separation Flow Control by the Gas Injection Contrary Supersonic Stream

Leonid A. Bazyma*
National Aerospace University, 61070 Kharkov, Ukraine
and
Vasyl M. Rashkovan†
National Polytechnic Institute, 04430 Mexico, D.F., Mexico

DOI: 10.2514/1.18497

The numerical modeling of the supersonic flow over the annular step body formed by two coaxial cylinders is performed within the ideal gas model framework through Godunov's method. The numerical simulation has shown that for the cylinder–cylinder configuration without cavity there exist two characteristic flow regimes, which follow one after the other periodically. The flow over the cup-cylinder configuration (without jet injection) has unsteady character also. Numerical calculations indicate that bow shock oscillations remain the same or decrease in amplitude to a cavity with annular injection depending on the injection intensity. The domain of the steady flow existence is established.

Nomenclature

a	=	sound speed
C	=	constant coefficient
c_x	=	drag coefficient
D	=	cylinder diameter
d	=	cup or needle diameter
d_1, d_2	=	annular wall jet outside and inside diameters
E	=	total energy per unit mass, $e + (1/2)\boldsymbol{q} \cdot \boldsymbol{q}$
Err	=	error
e	=	internal energy per unit mass
F_s	=	factor safety
f	=	solution value
h	=	grid spacing
k	=	injection parameter, $k = r_j u_j^2 / r_\infty u_\infty^2$
L	=	needle length
l	=	depth of the cavity
M	=	Mach number
p	=	pressure
p_c	=	empirical order of convergence
$\boldsymbol{q}$	=	velocity vector
Re	=	Reynolds number
r_r	=	refinement ratio
St	=	Strouhal number
s	=	axial distance from the cavity base to the mean shock position, $s = (l + \Delta)$; Fig. 1
t	=	time
u, υ	=	velocity vector ($\boldsymbol{q}$) components on the axes x and r
x, r	=	cylindrical coordinate system components
γ	=	ratio of specific heats
Δ	=	bow shock-wave average standoff distance from the rim of the cup or needle
δ	=	cup wall thickness
ρ	=	density
τ_x, τ_r	=	mean time intervals

Subscripts

j	=	jet parameters
fine	=	fine grid value
exact	=	exact value
∞	=	freestream flow conditions

Presented as Paper 5302 at the AIAA Atmospheric Flight Mechanics Conference and Exhibit, Austin, Texas, 11–14 August 2003; received 29 June 2005; revision received 10 June 2006; accepted for publication 16 September 2006.

*Ph.D., Associate Professor, "Kharkov Aviation Institute" (KhAI), Department 402, 17 Chkalov Street; bazyma@rambler.ru; bazima@htsc.kipt.kharkov.ua.

†Dr. Sc., Ph.D., Professor, National Aerospace University of Ukraine; Professor-Invitee of High-School of Mechanics and Electric Engineering of National Polytechnic Institute of Mexico, Colonia San Francisco Culhuacán, Avenue Santa Ana No. 1000, C.P. 04430, Mexico D.F.; vasyl@calmecac.esimecu.ipn.mx.

I. Introduction

A variety of supersonic and hypersonic vehicles, tactical and strategic hypersonic and supersonic missiles, and hypersonic cruise aircraft are of considerable commercial and military interest. All these vehicles are extremely sensitive to aerodynamic drag [1,2]. The combination of the two main rocket operation factors, low altitude and high velocity, produces considerable heat flows in the stagnation region of the nose [3–7]. For this reason, passive heat transfer analysis under such conditions is very important for understanding and solving rocket operation problems.

Recent analyses have shown that the nose-tip heat transfer can be reduced using a forward-facing nose-tip cavity [3–5,7] with minimal drag penalties. Additionally, a coaxially directed sensor can be installed in the bottom of these cavities [3,8]. The introduction of a forward-facing cavity can be used to delay ablation onset, without increasing drag, by slightly decreasing the nose-tip diameter [9].

It is well known that supersonic flow around bodies with cavities located on the nose is accompanied by pulsation [10–14]. A forward-facing cavity may be regarded as a resonance tube. One of the characteristics of a hollow-nosed missile at supersonic Mach number is an oscillating bow shock that can significantly influence missile drag, heat transfer, and signal propagation through the cavity [3]. The laser perturber has been used to investigate the effects of disturbances on various types of flowfields including stagnation regions on blunt bodies and forward-facing cavities [15].

Several methods of the bow shock stabilization have been considered. Flow stabilization by jet injection from the cavity bottom is discussed in previous work [13]. For example, the annular jet injection from the cavity bottom can stabilize the flow over the hollow cylindrical body (a cup) and reduce the amplitude of shock oscillations in front of the cavity produced by movement of the bow shock flow [13].

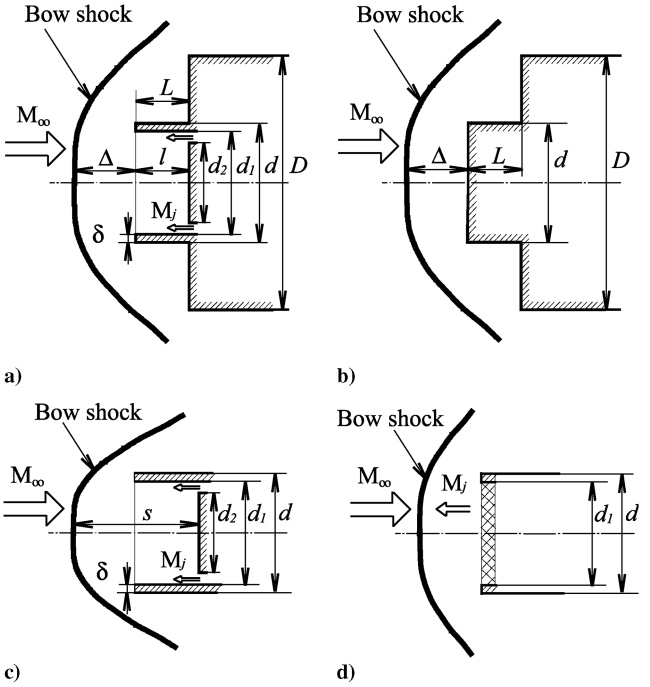

Fig. 1 Schemes of considered geometries.

The flow separation from the streamlined surface is the characteristic phenomenon, which accompanies liquid or gas motion. When separation occurs, the pressure redistribution along the vehicle takes place. Therefore, important integral characteristics, resistance and lift, change. In some cases separation is harmful: the efficiency reduction of the body carrier capacity, control worsening, thermal flow growth on some streamlined surface parts. When the separation control takes place, the required regulative forces and moments are created, the allowed regime of heat transfer is provided, and aerodynamic characteristics of the vehicle are improved [16].

More frequently, separated flows appear near various kinds of protrusion, superstructures, fractures, cavities, and incident shock wave falling onto the streamlined surface and the bodies of compound configuration. The separation flows around ailerons, interceptors, and wings on the supercritical angle of attack are also found. The flow separation can be jet influenced, when the devices, which control aerodynamic and gas-dynamic characteristics, function. One of the control methods for aerodynamic resistance of blunt bodies is the application of superstructures made, for example, in a needle shape or in a needle shape with a disk. Such constructions allow reducing a drag coefficient and considerable changing of the pressure center position of the body. Under some conditions the flow pulsations can appear on the surface of the fore part of the body. They reduce the needle application effect and impede the flow control. The efficiency of the control influence on the flow around blunt surfaces of vehicles can be greatly increased with the combined device of a cylindrical hollow needle for gas injection into the contrary flow. In the experiments conducted on the models with plane faces the pulsation character of the noninjection flow with all relative needle lengths is indicated. The gas injection (hydrogen) provided the stabilization influence and the pulsations disappeared. Higher combusting gas consumption led to pulsations again [16].

In the past few years, there has been considerable debate [17–19] regarding numerical pseudopulsations around blunt bodies. A perturbed grid test case proposed by Quirk [17] exposes an odd–even decoupling problem suffered by some flux solvers. In the blunt body problem, certain grids lead to carbuncle solutions while others do not [19]. Weak or mild shock instabilities may still be obtained by the following methods: AUSM-M (advection upwind splitting method scheme named as the Mach splitting version), AUSM+ (more recent variant of AUSM-M scheme), HLLC (Harten–Lax–van Leer–Einfeldt), Godunov, and Osher with the natural ordering [18]. Also known as Godunov-type schemes, exact Riemann solvers find the unique solution to a Riemann initial value problem defined by the left and right interface states. Although somewhat wasteful, exact Riemann solvers do produce accurate and (usually) well-behaved shock waves because of their close physical base [17].

The current work addresses the influence of the intensity jet injection on the supersonic flow stabilization and the aerodynamic resistance changes of the combined body configuration with needle and with a cylindrical cavity (cup mounted at the end of the round cylinder).

II. Problem Definition

Consider the problem of constant, axisymmetric flow around a cup-cylinder configuration ($L/d = l/d = 1.6$; $\delta/d = 0.04$; $D/d = 3.2$; $d_1/d = 0.92$; $d_2/d = 0.84$) with a uniform, ideal supersonic gas flow. The cup-cylinder configuration scheme is depicted in Fig. 1a.

This combined configuration can be considered as a body with a needle (Fig. 1b, $L/d = 1.6$; $D/d = 3.2$) and as a body with a forward cavity (Fig. 1c, $l/d = 1.6$; $\delta/d = 0.04$; $d_1/d = 0.92$; $d_2/d = 0.84$). It is known that the flow of such bodies can be nonstationary. Therefore each of these configurations will be considered separately from each other. Interaction of a jet with a freestream flow will be considered also (Fig. 1d, $\delta/d = 0.04$; $d_1/d = 0.92$; $d_2/d = 0$).

The equations of gas dynamics in the cylindrical coordinates have the form

$$\frac{\partial \rho r}{\partial t} + \frac{\partial \rho u r}{\partial x} + \frac{\partial \rho \upsilon r}{\partial r} = 0 \tag{1}$$

$$\frac{\partial \rho u r}{\partial t} + \frac{\partial (p + \rho u^2) r}{\partial x} + \frac{\partial \rho u \upsilon r}{\partial r} = 0 \tag{2}$$

$$\frac{\partial \rho \upsilon r}{\partial t} + \frac{\partial \rho u \upsilon r}{\partial x} + \frac{\partial (p + \rho \upsilon^2) r}{\partial r} = p \tag{3}$$

$$\frac{\partial \rho E r}{\partial t} + \frac{\partial \rho u (E + p/\rho) r}{\partial x} + \frac{\partial \rho \upsilon (E + p/\rho) r}{\partial r} = 0 \tag{4}$$

Equations (1–4) involve the system variables. The above system of equations is closed by the equation of state of the ideal gas

$$\rho E = p/(\gamma - 1) + (1/2)\rho \boldsymbol{q} \cdot \boldsymbol{q} \tag{5}$$

To use dimensionless values, we make use of the following equalities:

$$r = \bar{r}D/2, \quad x = \bar{x}D/2, \quad t = \bar{t}D/(2a_\infty), \quad a = \bar{a}a_\infty$$
$$u = \bar{u}a_\infty, \quad \upsilon = \bar{\upsilon}a_\infty, \quad \rho = \bar{\rho}\rho_\infty, \quad p = \bar{p}\rho_\infty a_\infty^2 \tag{6}$$

where a_∞ is the incident flow sound speed. In the following text, we have omitted bars above the dimensionless values r, x, t, a, u, υ, ρ, and p.

On the body surface and along the symmetry axis, solid-wall inviscid boundary conditions were applied. Along the external inflow boundary, undisturbed freesteam conditions were used. On the downstream outflow boundary, extrapolation of the flow quantities from the adjacent internal boundary was performed.

When the injection is in the body, we specify the conditions of the jet escape at the sound velocity $M_j = 1$ and outflow parameters $u_j = -1$, $\upsilon_j = 0$, $\rho_\infty = kM_\infty^2$, and $\gamma_j = 1.4$ similar to those in [13]. The jet parameters are sent to the corresponding grid cells at the surface of the body. The injection intensity $k = \rho_j u_j^2/\rho_\infty u_\infty^2$ is varied in the range of 0.5–1.5.

The initial data in calculations without injection corresponded to the dimensionless parameters of the incident stream:

$$p = p_\infty = 1/\gamma, \qquad \rho = \rho_\infty = 1, \qquad u = u_\infty = M_\infty, \qquad \upsilon = 0 \tag{7}$$

Subsequent solutions of the flow with injection were initialized using the flow solution without injection. The solutions were advanced in time until the average flow conditions were stabilized.

III. Numerical Method

The equation system solution (1–4) was conducted by Godunov's method [20] on a grid mesh uniform (60×70: for the cup cylinder, Fig. 1a, and for the needle cylinder, Fig. 1b; 100×40 and 60×40: for the hollow cylinder, Fig. 1c; 150×50: for the jet interaction, Fig. 1d), which was designed by densening the mesh point all around the body region, with the exception that in the cavity, the mesh points distribution was set to be uniform. The ratio of the grid cell side sizes in the cavity was $\Delta r/\Delta x = 0.4$ (24 nodes in the transverse and 33 nodes in the longitudinal direction). The results of the flow calculation over a cup for such a ratio are close to the experimental data of [12] for the $M_\infty = 3.7$ (for example, a difference between the numerical and experimental Strouhal number of no more than 5%). The calculations were performed using the same finite-difference scheme of the first-order approximation as that employed in [20]. The basis for such a choice is given below (see [13,21] also).

A. Stability Condition

The necessary and sufficient condition for stability is that the permissible spacing in time τ must satisfy the inequality

$$\frac{\tau}{\tau_x} + \frac{\tau}{\tau_r} \le 1 \tag{8}$$

that results from a stability study of Godunov's difference scheme realized on the system of nonstationary acoustic equations on a uniform rectangular (or parallelogram) grid. Here τ_x, τ_r are the time spacing of the one-dimensional scheme. Physically τ_x and τ_r are mean time intervals, in which waves, which appear at the break decomposition on the cell boundary, reach the neighboring boundaries:

$$\tau_x = \frac{\Delta x}{\max(u + a, a - u)}, \qquad \tau_r = \frac{\Delta r}{\max(\upsilon + a, a - \upsilon)} \tag{9}$$

The stability condition so given is extended to the quasilinear equations of gas dynamics. Calculations show that this condition (8) provides the necessary stability. Nevertheless, this condition is usually used with a right-hand side less than 1.

In the current work, the time step is chosen from cell to cell according to the stability condition as follows:

$$\tau_{n-\frac{1}{2},m-\frac{1}{2}} = \left(\frac{\tau_x \tau_r}{\tau_x + \tau_r}\right)_{n-\frac{1}{2},m-\frac{1}{2}}, \qquad \bar{\tau} = \min_{n,m} \tau_{n-\frac{1}{2},m-\frac{1}{2}} \tag{10}$$

In k space its value with respect to time is calculated using the following spacing $k + 1$:

$$\tau^{k+1} = K\bar{\tau}^k \tag{11}$$

where K is a safety factor that is similar in meaning to the Courant number.

B. Comparative Analysis

Computer simulation of many gas-dynamics problems of quite complex flow dealt with a model of an inviscid non-heat-conducting gas and difference schemes for start-to-finish calculation. Both steady and unsteady flows with more or less numerous strong and weak (including interacting) discontinuities are usually considered in this formation.

It is impossible [20] to achieve a combination of high resolution (minimum "blurring" of discontinuities transferred as regions of rapid parameter change) and monotonically of the solution (no numerical oscillations near discontinuities) on uniform linear schemes of any finite approximation order [20]. With monotony ensured, first-order approximation difference schemes intensively blur any discontinuities, due to high approximation viscosity. On the contrary, uniform linear schemes higher than first-order approximation give the best resolution (to weak discontinuities, in particular). But these schemes are nonmonotonous.

One of the best first-order schemes, the Godunov's one [22] provides good resolution of the gas-dynamics singularities through the exact solution of the nonlinear problem of arbitrary discontinuity decay of the gas-dynamic quantities on the calculation cell faces. Godunov's scheme is based on piecewise-constant parameter distribution within a cell and considerably blurs shock waves and contact discontinuities like all first-order schemes.

Problems of Godunov's scheme approximation order increase have been considered in many publications in recent years. The scheme approximation order can be increased by replacing the piecewise-constant parameter distribution for the piecewise-linear one. Kolgan [23] proposes to combine a piecewise-linear distribution with the minimum derivation principle (Kolgan's scheme loses its monotony in Euler's equations for strong discontinuities). Van Leer [24] has used his own minimum derivation principle version to construct quasimonotonous second-order schemes in Lagrangian and Euler coordinates. These approaches were developed further in [25–27].

In [25] a piecewise-parabolic parameter distribution is used on the lower layer. A modification of the minimum derivation principle for the Godunov–Kolgan scheme is proposed in [26] with a predictor–corrector procedure used in [27]. Although high order approximation schemes have obvious advantages (the blurring of contact discontinuities and weak shocks is much diminished), the parameter calculating procedure on cell lateral faces is quite complicated. Moreover, for flows containing strong gradients or discontinuities, higher-order interpolation techniques can instigate high frequency noise production and instability, and cause the CFD solver to generate incorrect solutions or fail completely. At the same time, algorithms intended for solving practical problems, and unsteady process simulation, in particular, must meet the demand for both accuracy and computational efficiency (calculation on relatively coarse grids, economy, and implementation simplicity).

Thus, the numerical model development on the base of nonstationary Euler equations with approximate dissipation mechanism is preferred in this work.

C. Grid Convergence Test

A grid convergence study is a method for determining the "ordered" discretization error in a CFD simulation and involves performing the simulation on two or more successively finer grids. The method results in an error band on the computational result which indicates the possible difference between the discrete and the continuum value.

Assessing the accuracy of codes and calculations requires that the grid is sufficiently refined such that the solution is in the asymptotic range of convergence, which is the range in which the discretization error reduces asymptotically with decreasing grid size.

The order of grid convergence is the order p in the relationship between the grid spacing h and the solution error Err, which is the difference between the discrete solution $f(h)$ and the exact solution f_{exact},

$$Err = f(h) - f_{\text{exact}} = Ch^{p_c} \tag{12}$$

where C is a coefficient.

The order of convergence p_c (see [28]) can be evaluated using the solutions at three grid levels with constant grid refinement ratio $r_r = h_3/h_2 = h_2/h_1$,

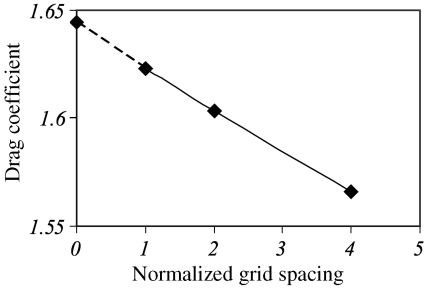

Fig. 2 The drag coefficient of the flat-face cylinder.

$$p_c = \ell_n\left(\frac{f_3 - f_2}{f_2 - f_1}\right) \Big/ \ell_n(r_r) \tag{13}$$

Richardson extrapolation is a method for obtaining a higher-order estimate of the continuum value (value at zero-grid spacing) of the solution f from a series of lower-order discrete values. A generalized Richardson extrapolation can be expressed for a noninteger refinement ratio r_r and order of convergence p_c as

$$f_{h=0} = f_1 + \frac{f_1 - f_2}{r_r^{p_c} - 1} \tag{14}$$

A grid convergence index (GCI), based on Richardson's extrapolation, has been developed to assist in the estimation of the grid convergence error [29]. The GCI on the fine grid h_1 is defined as

$$\mathrm{GC\,I_{fine}} = \frac{F_s|(f_2 - f_1)/f_1|}{(r_r^{p_c} - 1)} \tag{15}$$

The factor of safety is recommended to be $Fs = 3.0$ for comparisons of two grids and $Fs = 1.25$ for three or more grids.

The use of the above relations within a grid convergence study is demonstrated for a CFD simulation of the Mach 3.7 flow past a flat-face cylinder, of diameter and length equal to that of the needle nose configuration (Fig. 1b, $L/d = 1.6$). The objective is to evaluate the drag coefficient of the cylinder. The flowfield was computed on three grids, each with twice the number of grid points in each coordinate direction such that the grid refinement ratio was $r_r = 2$. Table 1 reports the values of a drag coefficient on each grid. Each simulation was checked for acceptable iterative convergence. The convergence criterion is based on the difference in density values, ρ, at any grid point between two successive iterations, that is, $|\rho_{n+1} - \rho_n| \le 10^{-5}$, where n is the iterative index. The periodicity in the flowfield is obtained after about 4000 iterations. The column indicated by "spacing" is the spacing normalized by the spacing of the finest grid.

Figure 2 shows the plot of drag coefficients with varying grid spacings. As the grid spacing was reduced, the pressure recoveries approached a zero-grid spacing value.

Equation (13) was applied to calculate the observed order of convergence as $p_c = 0.94$. Richardson's extrapolation was applied using the two finest grids with Eq. (14) to obtain an estimate of the value of the drag coefficient at zero-grid spacing, which yields $f_{h=0} = 1.64419$. This is plotted in Fig. 2 as a dashed line.

The grid convergence index for the fine grid solution was calculated from Eq. (15) to be $\mathrm{GCI_{fine}} = 1.64361\%$ using a factor of safety of $F_S = 1.25$. This variation is sufficiently low. Based on this study we could say that the drag coefficient for the flat-face cylinder is estimated to be 1.64419 with an error band of 1.164%.

Table 1 Grid convergence study

Grid	Normalized grid spacing	Drag coefficient
1	1	1.62286
2	2	1.60341
3	4	1.56624

IV. Results and Discussion

Predictions of the flowfield about bodies with and without a forward-facing cavity (Fig. 1) were obtained for a freestream Mach number of 3.7 with and without injection.

The comparisons of the data obtained through the finite-difference first-order approximation Godunov's scheme with the experimental results and calculation data of other authors were realized for verification of the numerical method adequacy to the physical problem statement.

A. Physical Interpretation of the Jet Interaction with the Contrary Supersonic Flow

Physical processes, which form the basis of jet operating control, differ in some common feature. When the gas is injected, the aerodynamic interference between the injection flow and main flow occurs, the separation flows appear, and their parameters change. That gives considerable pressure redistribution on the vehicle streamlined surface. Therefore, the control jet is means of separation flow control.

The gas injected into the contrary supersonic flow from the nozzle located in the vehicle critical point vicinity is an effective means of the frontal resistance control. The nozzle outlet section gas has velocity equal or even higher than sound speed and pressure normally higher than that in the contrary flow. The nozzle outflow is performed in the underexpansion regime. The injection pressure increase leads to the jet size widening and the bow shock-wave withdrawal from the body.

The injected flow has a barrel shape with typical flow elements for the underexpanded jet. The scheme of interaction between injected gas and the spatial axially symmetric flow is defined through the visual observation [30] (Fig. 3). The gas jet 3 separates from the sharp hole edges, reaches the general flow interface 6, and turns and flows around the head part 2 surface. The toroidlike stagnant zone 11 with the reverse flow appears inside the jet. The separation current lines 10 limit the zone. The jet mixes with both the contrary flow and the gas circulating in the stagnant zone and forms appropriate mixing areas 5 and 7. In the zone of the jet attaching to the streamlined surface (in the vicinity of the intersection point of separating current lines and the body) the curve-line shock wave 1 originates. The compound flow structured velocity relaxation zone 4 is formed beyond the attaching zone on the streamlined surface. Both the contrary flow and the jet have the common critical point 8 with equal braking pressure $p'_{0\infty} = p'_{0j} = p_0$ on the interface. When contrary flow braking occurs under pressure p'_{0j} immediately beyond the bow shock wave 12, the jet is broken to the pressure p'_{0j} beyond the shock wave 9 close to the normal one, which appears in front of the interface. With the contrary jet injected, pressure reduction on the frontal surface leads to the lower shock-wave drag coefficient c_{xv}. The shock-wave drag coefficient reduces when $n = p_j/p_\infty$ increases.

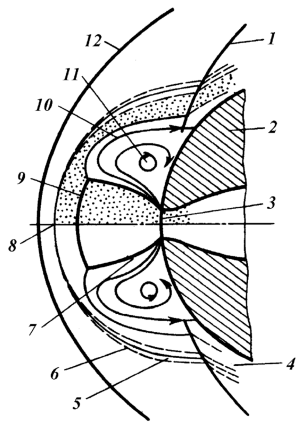

Fig. 3 Flow structure at interaction between underexpansion gas jet and the contrary supersonic flow.

Observed in Fig. 3 the current scheme with jet-flow interaction is not unique. Under certain conditions the structure of such a current can become unstable, and unfavorable pressure pulsations appear on the streamlined surface. The pulsation appearance mechanism is connected with the transition from the "unibarrel" jet form to the "multibarrel" periodical one. Such a current scheme accords to the conditions, when the underexpanded coefficient approaches to one. The underexpanded coefficient n reduction takes place due to the pressure increase in the stagnant zone p_d, which encompasses the jet ($n' = p_j/p_d$, p_j, pressure in the nozzle exit section). Its elongation accompanies the transition to the multibarrel structure of the jet. The total pressure losses in the jet diminish. It will cause bow shock wave great backward movement from the streamlined body and pressure reducing in the stagnant zone. If further off-design rising occurs, the jet will confirm the unibarrel form again, and its length will diminish. The bow shock wave will approach the surface again, the pressure p_d will rise, the underexpanded coefficient will reduce, etc. Such a process of pulsation origin occurs with considerable frequency of the order 10^{-1} s.

B. Simulation of Jet Interaction Processes with the Contrary Supersonic Flow

A number of characteristic similarity parameters are significant in the problems of jet interaction simulation. It is impossible to realize an equality of all the criteria in flight conditions. Therefore, the parameters, which determine the main effects of jet interaction, are chosen. To simulate the processes of jet and contrary flow interaction and their interferential influence on the streamlined surfaces of geometrically similar bodies such as the initial system of denominating quantities, the following parameters can serve: velocity, density, temperature, average molecular mass, specific thermal capacity of the undisturbed flow, characteristic body dimension, appropriate parameters of gas flow for the injected jet, and injection nozzle size. It is considered that among the 14 parameters only any four (for example, characteristic body dimension, velocity, temperature, and density) have independent quantity dimensions. Therefore, according to the π *theorem* of the general theory of quantity dimensions the considered phenomenon can be described by 10 nondimensional combinations—similarity parameters. The similarity condition cannot be satisfied for all the parameters in the simulation experiments, as a rule; therefore it is needed to define the most considerable top priority dependence of aerodynamic coefficients on one of the defined criteria of similarity. In the present transaction one can observe the outflow from the circular cylinder face. The body characteristic dimension (cylinder diameter) and the injection nozzle characteristic dimension (nozzle exit section diameter) are approximately equal to one another by value (Fig. 1d). Let $n = p_j/p_\infty$ and $k = \rho_j u_j^2/\rho_\infty u_\infty^2$ be added to the characteristic dimensions for any aerodynamic parameters M and γ.

The flow over a cylinder configuration (see Fig. 1d) by an ideal gas flow with the Mach number $M_\infty = 3.7$ is considered. When the injection exists on the aircraft body, the conditions of the jet flow with the sound velocity $M_j = 1$ is given. The injection intensity $k = \rho_j u_j^2/\rho_\infty u_\infty^2$ is accepted $k = 1.35$, and the underexpanded coefficient is $n = p_j/p_\infty = 18.5$.

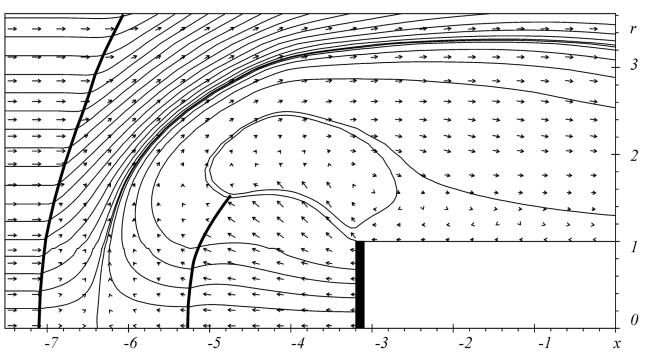

Fig. 4 Velocity vector field, streamlines, and shock-wave positions.

The velocity vector field and streamlines and shock-wave positions represented in Fig. 4 permit one to consider that the main structural elements of the jet-contrary flow interaction correspond well to the conception of such an interaction resulted from theoretical and experimental investigation (see Fig. 3).

Through theoretical and experimental investigations one can note that the jet operating control is the separation flow control means. When the gas is injected, the aerodynamic interference between the injection and main flows occurs, and the separation flows appear (Fig. 3). In this case their parameters change that give the considerable pressure redistribution on the vehicle streamlined surface. Gas jet injected into the contrary supersonic flow from the nozzle positioned in the proximity of the critical point of the vehicle is an effective means of the frontal resistance control. At that moment gas velocity in the nozzle outlet section is equal to or even higher than local sound speed and the pressure normally higher than that in the contrary flow. The injection pressure increase leads to the jet size widening and the bow shock-wave withdrawal from the body. The jet mixes with contrary flow and gas, which circulates in the stagnant zone, and appropriate mixing areas are formed. In the zone the jet attaching to the streamlined surface (in the proximity of the intersection point of separating streamlines with the body) the curve-line shock wave originates. The boundary layer with the compound flow structure is formed beyond the streamlined surface attaching zone. When the contrary flow braking occurs immediately beyond the bow shock wave, the jet is broken beyond the shock wave close to the normal one, which appears in front of the interface. The pressure reduction on the frontal surface with the contrary jet injected gives the lower shock-wave drag coefficient c_x.

C. Flow Around a Hollow Cylinder

Stable pressure pulses on the cavity bottom have been observed experimentally [12] at uniform supersonic flow around a hollow cylinder. The experimental results [11] were compared to the computer simulation [31] for $M_\infty = 3.7$, $l/d = 1.6$, $\delta/d = 0.04$ (see Fig. 1c), in which kinetically compatible difference schemes were used [31]. The calculation [31] was carried out on the space-uniform difference grid 81×81 ($\Delta x = 0.1$, $\Delta r = 0.02$). The cylinder radius was taken as the characteristic length. In the range of numbers $Re_\infty \geq 10^5$ where, according to [12], the Re_∞ influences the main process characteristics (average shock wave moving away, shock-wave pulsation amplitude, oscillation period) is not considerable, the strong correspondence with experimental data is obtained.

The flow around a hollow cylinder in the formulation of Yelizarova et al. [31] was examined. The results of calculations on rectangular immobile (60×40, 100×40) and mobile [21] (38×40, 65×40) grids were compared.

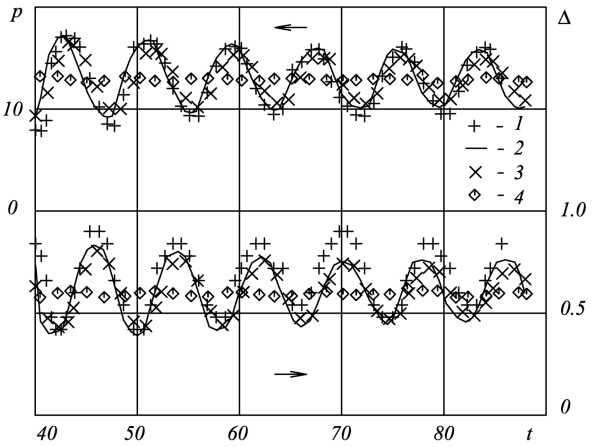

Fig. 5 Pressure variation in the center of the cavity bottom and the bow shock wave average standoff distance: 1—100 × 40 fixed grid, Godunov's scheme [20]; 2—81 × 81 fixed grid, [31]; 3—38 × 40 mobile grid, modified scheme [21]; 4—38 × 40 mobile grid, Godunov's scheme [20].

Table 2 Process main features

Δ^0	Δ^*	St	Grid size ($K \times M$)	Difference scheme
0.3	0.08	0.246	81×81 (fixed)	Yelizarova et al. [31]
0.33	0.12	0.252	100×40 (fixed)	Godunov
0.3	——	——	38×40 (mobile)	Godunov
0.32	0.09	0.251	38×40 (mobile)	Modified Godunov [21]
0.4	0.3	0.237	60×40 (fixed)	Godunov
0.3	——	——	65×40 (mobile)	Godunov
0.3	0.07	0.250	65×40 (mobile)	Modified Godunov [21]

The mobile grid calculations were realized through both Godunov's method [21] and the modified Godunov's scheme in Bazyma and Kholyavko's [21] formulation.

The calculation results on the 100×40 fixed grid are in good agreement with Yelizarova et al. [31] results. Figure 5 shows the time-dependent pressure change ($p/p_\infty\gamma$) at the cavity bottom center and the shock-wave withdrawal from the cylinder section (1 for 100×40 Godunov's scheme, 2 for the Yelizarova et al. [31] result). The average shock-wave withdrawal $\Delta^0 = \Delta/d$, pulsation amplitude $\Delta^* = \Delta'/d$, and Strouhal number $St = s/(a_0 t^0)$ for different variants are given in Table 2 ($St \approx 0.25$, $\Delta^0 \approx 0.3$–0.45, $\Delta^* \approx 0.1$–0.3 in the experiment [12]). Here t^0 is the oscillation period, a_0 is the stagnation temperature sound velocity, and $s = (l + \Delta)$ is the characteristic length (Fig. 1c).

The mobile 65×40, 38×40 grid calculations through Godunov's scheme [32] showed that by the time $t \approx 40$ the cavity pressure pulses had decayed (Fig. 5, 4—38×40 grid, Godunov's scheme). However, the modified Godunov's scheme [21] picked out oscillations (Fig. 5, 3—38×40 grid), with the process main features (see Table 2) corresponding both to the calculation [31] and the experiment [12].

The datum comparison obtained in calculations on different grids showed their good qualitative similarity. The difference lies in pulsation amplitude values and the average shock wave moving away. It is connected with the viscosity approximation influence which depends on both the flow structure and the calculation grid geometry.

Further calculations are fulfilled on fixed grids in order to reach the maximum reduction of the numerical effect influence on the obtained results.

Wall annular jet injection calculations ($d_1/d = 0.84$, $d_2/d = 0.92$, Fig. 1c) from the hollow cylinder bottom (grid size 100×40) were also fulfilled. The jet intensity varies in the range of $k = 0.5$–1.5. The fields of gas-dynamic parameters obtained in noninjection calculation at the time $t = 51$ are used as the initial data.

The annular jet injection orients the velocity vector in the hollow wall region toward the contrary flow. The pressure pulsation attenuation takes place at the injection intensity $k = 0.5$ (Fig. 6). Up to the values $k \approx 1$ the flow is stationary, and the shock wave moving away rises ($\Delta^0 \approx 0.55$). The further injection intensity increase ($k = 1.5$) leads to the jet-shock wave interaction resulting in nonstationary flow. As results show one can control the pulsation process through the wall annular jet injection intensity regulation.

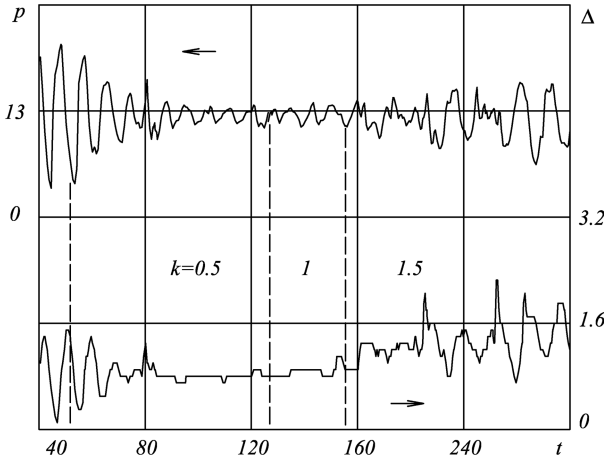

Fig. 6 The pressure variation in the cup bottom center.

D. Flow over the Cylinder–Cylinder Configuration

Flow over the nose-needle cylinder will be unsteady if the needle length to the cylinder diameter ratio corresponds to the cup length to the cylinder diameter ratio considered in this work $L/D = 0.5$. The flow over the needle-cylinder configuration is also determined by the needle diameter to the cylinder one ratio and the needle geometry. Conic or cylindrical bodies (sharpened, spherically blunted, or flat ended, but nonrecessed) have been used as needles. The flow character over the considered cup-cylinder configuration will be also determined not only by unsteady recess processes but also by the cup length and diameter to the cylinder diameter ratios (L/D and d/D). However, there are no scientific data on the needle-cylinder flow with a "relative" diameter d/D corresponding to the relative cup diameter considered in this work. One can note that "thin" needles ($d/D \approx 0.1$) were considered in unsteady flow over needle-body studies. One can make the preliminary calculation for the cylinder–cylinder configuration (we replaced the cup by the solid cylinder with the same length and diameter as those of the cup). The flow over the cylinder–cylinder configuration has an unsteady nature and is comparable to the flow over the short needle cylinder. Papers on needle-body flows are reviewed in [16].

Figure 7 gives the calculation region fragments of the streamline location change depending on time. One can see that the flow of the larger diameter cylinder end vicinity is detached. The flow separation point on the smaller cylinder lateral surface passes below its rim. The well-developed region of the recirculation flow is formed in the larger cylinder end vicinity and the smaller cylinder lateral surface. The flow attaching point at the end is below the larger cylinder leading edge. The pulsations have a diverging character like those over the needle body. They arise from balance disruption between the gas thrown into the recirculation zone at the attachment point and the gas leaving the recirculation zone.

The experiments [33] have shown that there exist two flow regimes that differ in the recirculation region shape change character during pulsations, the average pressure values and heat fluxes to the body surface, and the pressure oscillation spectral characteristics. The flow regime without the noticeable change in the shape of the stagnant zone is called the regime of the first kind by Antonov and Gretsov [33]. The other regime with strong changes in the shape of the recirculation zone is called the regime of the second kind. In the transition from the first to the second regime the pressure and its distribution character over the body surface change abruptly. For the cylinder–cylinder configuration one can also distinguish two characteristic flow regimes, which follow one after the other periodically. Figure 7 shows the streamline positions at the time before and after the first to the second regime transition. Before the transition (fragment 1) the stagnant zone volume varies a little, and it remains approximately conic, although its boundary becomes convex or concave from time to time. The separation point positions

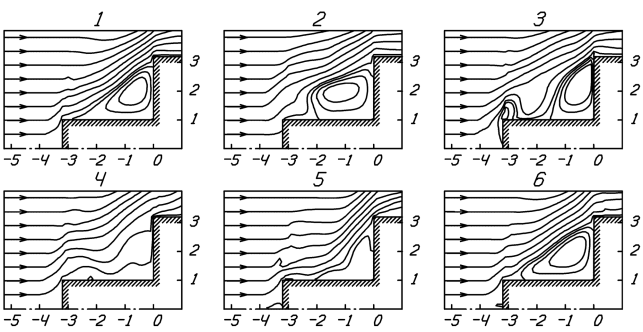

Fig. 7 Time variation of the location of streamlines in the flow over the cylinder–cylinder configuration: t = 80.8, 83.8, 84.4, 85.0, 87.6, and 91.3 (fragments 1–6, respectively).

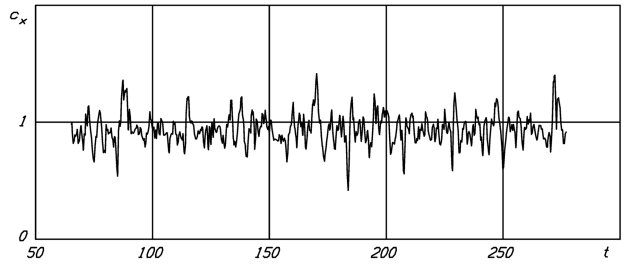

Fig. 8 The time variation of the cylinder–cylinder configuration drag coefficient.

also oscillate with low amplitude. The drag coefficient c_x of the cylinder–cylinder configuration in this flow regime varies in the range of 0.65–1.15. After the transition (fragments 2–4) the flow separation point shifts toward the larger diameter cylinder end, the stagnant zone boundary becomes convex, and its volume decreases. By the time $t = 85.0$ (fragment 4) it breaks up with a new stagnant zone formed (fragments 5, 6). This flow regime drag coefficient varies in the range of 0.5–1.4.

The second flow regime duration (the old stagnant zone breakup process and the new one formation) is $\Delta t_2 \approx 9$, which is considerably less than the first flow regime duration. Figure 8 shows the time variation of the cylinder–cylinder configuration drag coefficient. The maximum amplitude values c_x corresponding to the stagnant zone breakup and formation are observed in the time interval $\Delta t_1 \approx 80$–100. The calculation was done till $t \approx 500$.

E. Flow over the Cup-Cylinder Configuration Without Jet Injection

The flow over the cup-cylinder configuration (without jet injection) has unsteady character. As the flow over a cup [12,13] behaves, stable pressure and density pulsations are observed in the recess. The main process characteristics, the shock-wave average standoff distance, the pressure pulsation amplitude, and the oscillation period, are close to the calculated [13] and experimental data [12]. Figure 9 gives the pressure variation in the cup bottom center. The crosses mark the calculated results for the flow over the cup obtained in [13] on the 60×40 grid. The oscillations are

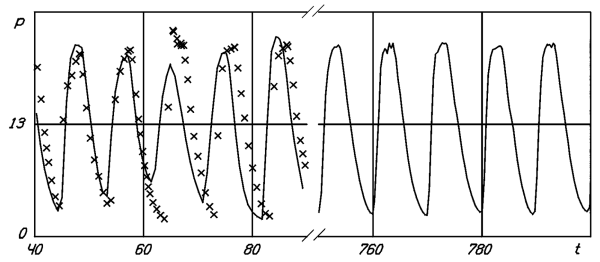

Fig. 9 The pressure variation at the cup bottom center: solid curves for the flow over the cup-cylinder configuration; crosses are for the flow over the cup.

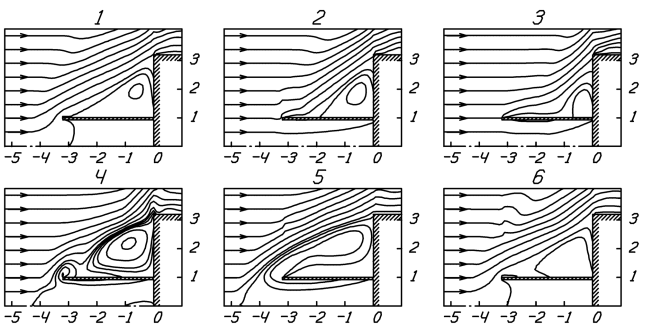

Fig. 10 The time variation of the streamline location in the flow over the cup-cylinder configuration: $t = 778.8$, 780.2, 781.7, 784.2, 786.9, and 788.3 (fragments 1–6, respectively).

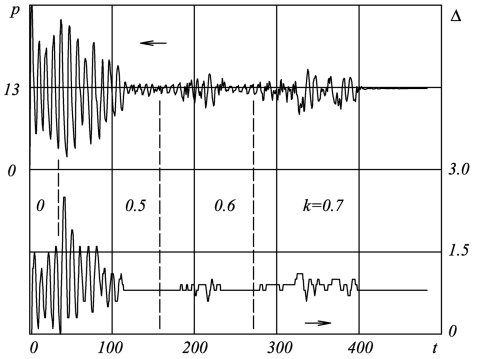

Fig. 11 The pressure variation in the cup bottom center.

established at time $t \approx 750$. The Strouhal number in the steady regime is $St = s/a_0 t^0 \approx 0.22$ [t^0 is the oscillation period, a_0 is the stagnation temperature sound speed, $s = (l + \Delta)$ is the characteristic length, and Δ is the bow shock-wave average standoff distance from the cup rim]. $St \approx 0.237$ is obtained in [13] for the cup flow on the same grid.

The stagnant zone shape in the cylinder end vicinity undergoes significant changes in the pulsation process. Figure 10 shows the streamline position variations over one oscillation period. Before the onset of the gas flow into the recess (fragment 1), the stagnant zone shape is approximately conic, its boundary is convex, the flow separation point lies on the cup lateral surface in the vicinity of its rim, and the attaching point lies on the cylinder edge. When the gas inflows into the recess, the stream separation point shifts from the cup rim toward the cylinder end, while the stagnant zone volume considerably reduces (fragments 2 and 3).

With the gas flow out of the recess, the stagnant zone volume increases and the separation and attaching points shift toward the cup and cylinder rims, respectively (fragment 4). The gas jet flowing out of the recess then merges with the stagnant zone (fragment 5). After the recess pressure drop (fragment 6) gas outflow finishes and a new cycle begins. During the pulsations, the cup-cylinder configuration drag coefficient c_x varies in the range of 0.5–1.8.

F. Flow over the Cup-Cylinder Configuration with Jet Injection

The annular jet injection directs the velocity vector in the boundary region near the recess wall opposite to the oncoming stream, which favors pulsation damping in the supersonic gas flow over the cup. A series of calculations of the flow over the cup-cylinder configuration with injection of an annular wall different intensity jet from the recess bottom is performed. The injection intensity was increased with the spacing $\Delta k = 0.1$ in the range of $k = 0.5$–0.7. Pressure variations at the cup bottom center and in the shock-wave standoff distance Δ from the cup rim (normal to the cup

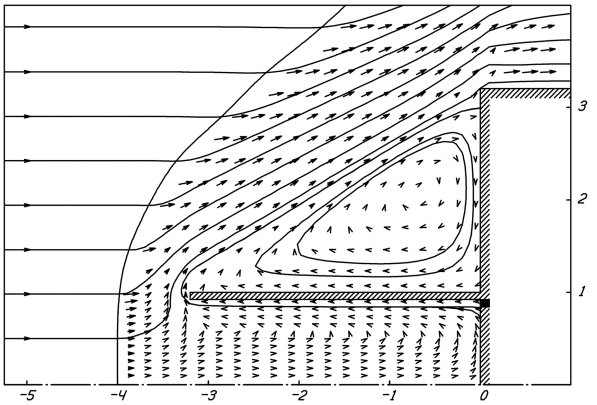

Fig. 12 Velocity vector field, streamline, and shock-wave positions in the steady regime ($k = 0.7$) for the cup-cylinder configuration with an annular wall jet injection from the recess bottom.

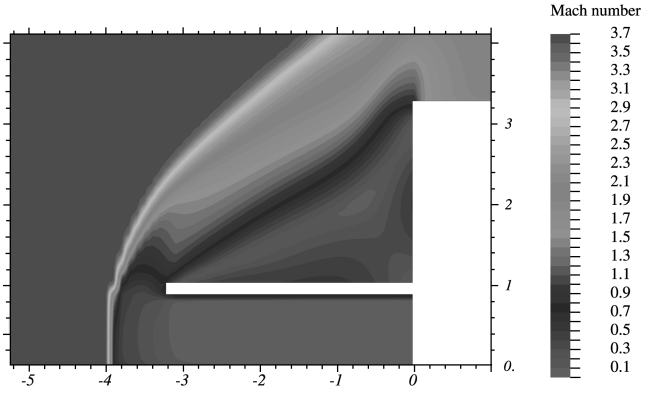

Fig. 13 Mach number isolines in the steady regime ($k = 0.7$) for cup-cylinder configuration with an annular wall jet injection from the recess bottom.

radius) as functions of the injection intensity are similar to the character of these parameter variations obtained in [13]. At injection intensity $k = 0.5$–0.6 for example, the considerable pressure pulsation amplitude decrease is observed, while at $k = 0.7$ the steady regime pressure variation at $t > 400$ was less than 0.001%. The bow shock standoff distance from the cup rim $\Delta = 0.8$ does not change with the injection parameter k variation.

The pressure variation in the cup bottom center and the shock wave moving away from the cup edge Δ (the ratio of the shock wave moving away distance to the cup radius) were presented in Fig. 11.

Figures 12 and 13 show the fragment of the calculation region for the injection intensity $k = 0.7$. The well-developed region of the recirculation flow in the cylinder edge vicinity and the cup lateral surface is observed. The flow attaching point lies at the cylinder end, below its edge. Further injection intensity increase leads to the attaching point shift towards the cylinder end edge. At $k > 0.875$ it was impossible to obtain a steady solution. When the attaching point approaches the cylinder end edge, the system sensitivity to any kind of perturbation increases.

This can disrupt the balance between gas entering the return-circulation flow region and gas leaving it and induce pulsations. With the injection intensity k variation in the range of 0.7–0.875, the cup-cylinder configuration drag coefficient c_x has steady flow regime values (see Table 3).

V. Conclusions

A numerical investigation of unsteady supersonic flow about nose tips with a forward-facing cavity was presented. The geometries of the investigation consisted of a needle-cylinder body with a cylindrical cavity (cup mounted at the end of the round cylinder). This combined configuration can be considered and as a body with a needle and as a body with a forward cavity. It is known that the flow of such bodies can be nonstationary. Therefore each of these configurations will be considered separately from each other.

The main pulsation characteristics in the cavity of the considered configuration are comparable to those obtained in the experiment and other calculations for the flow over the cup.

Over the cup-cylinder configuration (without injection) flow unsteadiness occurs due to recess pulsations and the recirculation zone pulsations in the cylinder end vicinity. The recirculation zone pulsations are coordinated with those in the recess, in contrast to the recirculation zone pulsations in the flow over the nonrecess configuration, where the two pulsation regimes periodically following one another are observed.

Table 3 Drag coefficient variation

k	0.700	0.750	0.800	0.850	0.875
c_x	0.731	0.724	0.719	0.714	0.712

The annular wall jet injection from the cavity bottom leads to the considerable decrease of pulsation amplitude for $0.5 \leq k < 0.7$. The steady flow pattern is observed in the injection intensity range of $k = 0.7$–0.875. With the further injection intensity increase with calculations up to $k = 1$, the pulsations occur again that are associated with the recirculation zone instability when the flow attaching point approaches the cylinder end edge.

The results from this work show that a jet injection can be used as an effective supersonic flow control method for space vehicles with needles and forward-facing cavities.

References

[1] Bushnell, D., "Supersonic Aircraft Drag Reduction," AIAA Paper 90.1596, June 1990.

[2] Ruffin, S. M., Gupta, A., and Marshall, D., "Supersonic Channel Airfoils for Reduced Drag," *AIAA Journal*, Vol. 38, No. 3, March 2000, pp. 480–486.

[3] Huebner, L. D., and Utreja, L. R., "Mach 10 Bow-Shock Behavior of a Forward-Facing Nose Cavity," *Journal of Spacecraft and Rockets*, Vol. 30, No. 3, 1993, pp. 291–297.

[4] Ycceil, K. B., and Dolling, D. S., "Nose Cavity Effects on Blunt Body Pressure and Temperatures at Mach 5," *Journal of Thermophysics and Heat Transfer*, Vol. 9, No. 4, 1995, pp. 612–619.

[5] Sarohia, V., and Back, L. H., "Experimental Investigation of Flow and Heating in a Resonance Tube," *Journal of Fluid Mechanics*, Vol. 94, No. 5, 1979, pp. 649–672.

[6] Burbank, P. B., and Stallings, R. I., "Heat-Transfer and Pressure Measurements on a Flat-Face Cylinder at a Mach Number Range of 2.49 to 4.44," NASA TM TMX-221, 1959.

[7] Engblom, W. A., Golbstein, D. B., Ladoon, D., and Schneider, S. P., "Fluid Dynamics of Hypersonic Forward-Facing Cavity Flow," *Journal of Spacecraft and Rockets*, Vol. 34, No. 4, 1997, pp. 437–444.

[8] Sambamurthi, J. K., Huernbner, L. P., and Utreja, L. R., "Hypersonic Flow over a Cone with a Nose Cavity," AIAA Paper 87-1193, 1987.

[9] Silton, S. A., and Goldstein, D. B., "Use of an Axial Nose-Tip Cavity for Delaying Ablation Onset in Hypersonic Flow," *Journal of Fluid Mechanics*, Vol. 528, April 2005, pp. 297–321.

[10] Bochachevsky, I. D., and. Kostoff, R. N., "Supersonic Flow over Convex and Concave Shapes with Radiation and Ablation Effects," *AIAA Journal*, Vol. 10, No. 8, 1972, pp. 1024–1031.

[11] Ladoon, D. W., Schneider, S. P., and Schmisseur, J. D., "Physics of Resonance in a Supersonic Forward-Facing Cavity," *Journal of Spacecraft and Rockets*, Vol. 35, No. 5, 1998, pp. 626–632.

[12] Antonov, A. N., and Shalaev, S. P., "Experimental Investigation of Unsteady Flow in Recesses in a Supersonic Flow," *Izvestya Academii Nauk USSR, Mekhanika Zhidkosti i Gaza*, No. 5, 1979, pp. 180–183 (in Russian).

[13] Bazyma, L. A., "Interaction Between Axial and Annular Jets Leaving a Cylindrical Cavity and an Incoming Supersonic Gas Flow," *Journal of Applied Mechanics and Technical Physics*, Vol. 36, No. 3, 1995, pp. 381–384 (translated from *Pricladnaya Mekhanika i Tekhnicheskaya Phyzica*, Vol. 36, No. 3, 1995, pp. 69–73).

[14] Bazyma, L. A., and Rashkovan, V. M., "Stabilization of Blunt Nose Cavity Flows by Using Energy Deposition," *Journal of Spacecraft and Rockets*, Vol. 42, No. 5, 2005, pp. 790–794.

[15] Schmisseur, J. D., Collicott, S. H., and Schneider, S. P., "Laser-Generated Localized Freestream Perturbations in Supersonic and Hypersonic Flows," *AIAA Journal*, Vol. 38, No. 4, 2000, pp. 666–671.

[16] Bazyma L. A, "Aerodynamics of Bodies of Revolution with a Front Separation Zone," Kharkov, Deposited at VINITI, 10.03.88, No. 7262-V88, 1988 (in Russian).

[17] Quirk, J. J., "A Contribution to the Great Riemann Solver Debate," *International Journal for Numerical Methods in Fluids*, Vol. 18, No. 6, 1994, pp. 555–574.

[18] Dumbser, M., Moschetta, J. M., and Gressier, J., "A Matrix Stability Analysis of the Carbuncle Phenomenon," *Journal of Computational Physics*, Vol. 197, No. 2, 2004, pp. 647–670.

[19] Chauvat, V., Moschetta, J.-M., and Gressier, J., "Shock Wave Numerical Structure and the Carbuncle Phenomenon," *International Journal for Numerical Methods in Fluids*, Vol. 47, No. 8-9, 2005, pp. 903–909.

[20] Godunov, S. K. (ed.), *Numerical Solution of Multidimensional Problems in Gas Dynamics*, Nauka, Moscow, 1976 (in Russian).

[21] Bazyma, L. A., and Kholyavko, V. I., "A Modification of Godunov's Finite Difference Scheme on a Mobile Grid," *Computational Mathematics and Mathematical Physics*, Vol. 36, No. 4, 1996,

pp. 525–532 (translated from *Zhurnal Vychislitelnoy Mathemetiki I Mathematicheskoy Fiziki*, Vol. 36, No. 4, 1996, pp. 124–133).

[22] Godunov, S. K., "A Difference Method for the Numerical Computation of Discontinuous Solutions of the Gas Dynamics Equations," *Matematichesky Sbornik*, Vol. 47, No. 3, 1959, pp. 276–306 (in Russian).

[23] Kolgan, V. P., "The Use of the Principle of Minimal Values of the Derivative to Construct Finite-Difference Schemes for Computing Discontinuous Solutions of Gas Dynamics," *Uchenye zapiski TSAGI*, Vol. 3, No. 6, 1972, pp. 68–78 (in Russian).

[24] Van Leer, B., "Towards the Ultimate Conservative Difference Scheme. V. A Second Order Sequel to Godunov's Methods," *Journal of Computational Physics*, Vol. 32, July 1979, pp. 101–136.

[25] Corella, P., and Woodward, P. R., "The Piecewise Parabolic Method (PPM) for Gas-Dynamic Simulations," *Journal of Computational Physics*, Vol. 54, No. 1, 1984, pp. 174–201.

[26] Tillyayev, N. I., "Generalization of a Modified Godunov's Scheme to Arbitrary Irregular Grids," *Uchenye Zapiski TSAGI*, Vol. 17, No. 2, 1986, pp. 18–26 (in Russian).

[27] Rodionov, A. V., "A Method of Increasing the Accuracy of Godunov's Scheme," *Zhurnal Vychislitelnoy Mathemetiki I Mathematicheskoy Fiziki*, Vol. 27, No. 6, 1987, pp. 1853–1860 (in Russian).

[28] Roache, P. J., "Need for Control of Numerical Accuracy," *Journal of Spacecraft and Rockets*, Vol. 27, No. 2, 1990, pp. 98–102.

[29] Roache, P. J., "Perspective: A Method for Uniform Reporting of Grid Refinement Studies," *Journal of Fluids Engineering*, Vol. 116, Sept. 1994, pp. 405–413.

[30] Krasnov, N. F., Koshevoy, V. N., and Kalugin, V. T., *Aerodynamics of Separation Flows*, Vishaya Shkola, Moscow, 1988 (in Russian).

[31] Yelizarova, T. G., Chetverushkin, B. N. and Sheretov, Yu. V., "Some Results of the Calculation of Supersonic Flow Past a Hollow Cylinder, Using Kinetically Compatible Difference Schemes," Preprint No. 97, Institute Prikladnoy Matememathiki Akademii Nauk, U.S.S.R., Moscow, 1989 (in Russian).

[32] Bazyma, L. A., and Rashkovan, V. M., "On Numerical Simulation of Supersonic Flow Using Bow-Shock-Fitting Technique," *Proceedings of ICFDP7: Seventh International Congress on Fluid Dynamics and Propulsion*, Sharm el-Sheikh, Sinai, Egypt, DC, 2001, pp. 1–7.

[33] Antonov, A. N., and Gretsov, V. K., "Unsteady Separated Supersonic Flow over Pointed and Spiked Bodies," *Fluid Dynamics*, Vol. 9, No. 4, 1974, pp. 578–582 (translated from *Izvestya Academii Nauk USSR, Mekhanika Zhidkosti i Gaza*, No. 4, 1974, pp. 93–99).

S. Aggarwal
Associate Editor